Vibration of locally cracked pre-loaded parabolic arches

Uğurcan Eroğlu[a,b], Giuseppe Ruta[b,c,*], Ekrem Tüfekci[d]

[a] *MEF University, Istanbul, Dept. of Mechanical Engineering*
[b] *University "La Sapienza", Roma, Dept. of Structural and Geotechnical Engineering*
[c] *National Group for Mathematical Physics*
[d] *Istanbul Technical University, Faculty of Mechanical Engineering*

Abstract

We study linear dynamics of an initially parabolic arch deformed by a uniform 'dead' load. The arch is seen as a fully deformable one-dimensional continuum with rigid cross-sections, one of which suffers from a small local crack at its boundary. The crack is simulated by springs, the stiffnesses of which are evaluated via stress intensity factors. By two first-order perturbations we investigate a non-trivial equilibrium adjacent to the reference configuration and small vibration superposed on it. The modulation of the initial load on the natural angular frequencies and its consequences on damage detection is described and commented. It turns out that neglecting the initial load, recalling for actual 'dead' structural actions, can be misleading in damage identification, while its inclusion leads to better results.

Keywords: vibration, arches, damage, initial load

2010 MSC: 74G10, 74H10, 74K10

---

1. Introduction

Structural damage may have several sources, from interaction with hostile environment to cyclic loading. Damage identification at an early stage is essential to: a) design possible maintenance and/or restoring interventions; b) prevent

*Corresponding author

Email addresses: `erogluug@mef.edu.tr`, `ugurcaneroglu.guest@uniroma1.it` (Uğurcan Eroğlu), `giuseppe.ruta@uniroma1.it` (Giuseppe Ruta), `tufekcie@itu.edu.tr` (Ekrem Tüfekci)

possible catastrophic failures due to the progressive reduction in local/global stiffness and bearing capacity. Several methods were proposed, focussing either on local inspection of the considered structure or on the assessment of its global behaviour [1, 2], i.e., its natural frequencies and mode shapes, which provide indirect information about the geometry, boundary conditions and material properties. For large civil structures and/or machinery under operation it was proved that the assessment of the structural global behaviour is more advantageous over techniques that focus on local investigations in terms of both time and cost [3]. Resorting to determining the structural dynamics, on the other hand, requires a detailed enough mathematical model of the examined structure and of its possible damages, to understand how they affect the response.

Models of cracks and crack-like damages in one-dimensional structural members date back to Kirshmer [4] and Thomson [5] in mid-20th century. They described the effect of a crack on the transverse dynamics of Euler-Bernoulli beams by considering any damaged element as composed by two chunks joined by a rotational spring that simulates the loss in bending rigidity caused by the crack. The stiffness of the spring was related to a characteristic length that provides a measure of the severity of the crack. However, more accurate evaluations for this fictitious stiffness had to wait until the publication of Irwin's paper [6], where we find the concept of *Stress Intensity Factor* (SIF) as a global, though coarse, quantitative measure of the intensity of crack-like damages of different shapes. This concept was used in many fields of engineering and applied sciences, especially after the handbook by Tada *et al.* [7], where we find SIFs for many cases. Their use goes along with 2nd Castigliano's theorem when we wish to model beam-type structures with damages, widening Kirshmer and Thomson's original idea. Following this approach, the sole rotation spring joining the beam regular chunks must be replaced by a set of springs, the effect of which is represented by a compliance matrix. Indeed, since coupling between axial and bending deformations is possible in presence of a crack [8], we need to represent at the same time transverse and axial local compliances due to the crack. In a linear setting, this is represented by a matrix, originally introduced by Dimaragonas and co-workers [8, 9, 10, 11, 3, 12, 13, 14, 14, 15, 16]. As for later studies, without pretending to be exhaustive, we may quote [17, 18, 19, 20, 21, 22]. We may refer the interested readers to the early review article by Doebling *et al.* [1] and to the recent review by Hou and Xia [23].

The majority of studies on damaged one-dimensional structural elements is devoted to straight beams, while there are relatively few investigations on curved beams and arches, which may also be seen as one-dimensional continua [24, 25]. One of the earliest of works is due to Dimaragonas [9], where the stability of rings with a transverse crack is examined. Krawzcuk and Ostachowicz [26] provided a finite element formulation for free vibration of cracked circular arches. Cerri and Ruta [27] presented analytical solutions to frequency shifts in doubly-hinged circular arches due to a crack. Subsequently, they also considered the identification of a crack by frequency data, and verified the procedure they proposed by comparisons with experimental data and using a richer one-dimensional model [28]. Viola et al. [29] applied both analytical and numerical methods to model shear-deformable circular beams with cracks. Later, Viola et al. [30] applied a similar approach to examine stepped circular arches. Karaagac et al. [31] used finite elements to investigate stability and dynamics of circular beams with an edge crack; to this aim, they used the specific SIFs for curved beams in [32] to distinguish from other studies. Caliò *et al.* [33] found the eigenproperties of circular shear-deformable arches where the damage is seen as a reduction of the cross-section stiffness properties; they presented a numerical technique for empowering their model in [34]. Cannizzaro *et al.* [35] used the properties of Dirac's delta to find the static response of purely flexible circular arches affected by several local cracks. Pau *et al.* [36] studied the inverse problem in a parabolic arch with a crack, proposing an objective function based on the variations of natural frequencies. Greco and Pau [37] examined statics of parabolic arches, concluding that for crack identification it is more advantageous to use approaches based on modal behaviour than those relying on the static response. Zare [38] performed an experimental modal analysis on cracked circular specimens for comparison with the results of the differential quadrature method, in which the crack is modelled by a rotational spring. Evolutionary algorithms are used by Greco et al. [39], and Eroğlu and Tüfekci [40] for damage identification in curved beams. Most researchers performed such studies dividing the beam in two regular chunks joined by a rotation spring, the stiffness of which is determined either directly by reduction of inertia of the cross-section or by the concepts of fracture mechanics. In both cases, the coupling between axial and bending strains due to a crack on the outer surface of the arch, which locally shifts the position of the neutral axis, is left out. However, the initial curvature of arches implies coupling also between axial force and shear force, and shear force and bending couple are coupled because of balance; hence, the additional coupling due to crack plays an important role in the arch response. Eroğlu and Tüfekci [40] highlighted that it may be possible to find crack location on the cross-section by introducing a non-material parameter linked to couplings. These were further investigated by the same approach in Eroğlu et al. [41] for parabolic arches; it is found that neglecting the coupling due to crack may be misleading in identification problems, especially for shallow arches. The position of the crack on the cross-section is further examined in [42] for static problems, and in [43] for stability problems of parabolic arches.

Great research efforts over the years found only little application on real structures, mainly because small local cracks slightly alter the natural frequencies, the detection of which is often soiled by noise and/or changes due to environmental effects, as pointed out also in [23]. In order to enrich the description of the actual behaviour of cracked structural elements, it might be required to account for the presence of 'dead' loads [44] or thermal effects [45] among possible sources of a non-trivial response. Motivated by this, in this work we take into account the effect of a simple pre-load on the natural angular frequencies of small vibration of parabolic arches affected by a small damage at the boundary of a cross-section. We first find the response of the arch to a 'dead' line load uniform along the span, assuming that the displacements of the axis and the cross-section rotations are small enough to linearise about the initial stress-free configuration. We then perform another first-order perturbation about the deformed shape, again supposing small kinematics, and search for a time-harmonic transverse response. The crack-induced couplings are represented by off-diagonal terms in the compliance matrix of the cracked section; their change in sign describes the crack location on opposite borders of the cross-section. We investigate the effects of the crack locations (along the axis and on opposite sides of the cross-section) and depth on the natural frequencies, which are modulated by the pre-load. After a verification, numerical results are obtained via the so-called principal matrix method, and are presented by several graphics, together with the relevant physical interpretations and thorough comments.

Sect. 2 presents the one-dimensional continuum model and the two first-order perturbations leading to the field equations for non-trivial equilibria and the superposed small vibration; Sect. 3 specializes the method to parabolic arches and reduces the governing equations into a non-dimensional form suitable for a resolution via the so-called transfer, or principal, matrix; Sect. 4 presents how a local small crack, represented by SIFs, affects the perturbed field equations; Sect. 5 presents a validation of the obtained equations; section 6 presents the numerical technique; Sect. 7 presents some results with extensive comments; a final section contains concluding remarks and open questions.

2. A one-dimensional model for plane arches

We see arches as one-dimensional structured continua: their shapes consist of copies of a plane figure (cross-sections) attached to the points of a portion of a regular plane curve (axis), referred to a Cartesian frame x, y and a consistent basis of unit vectors $\{\mathbf{e}_x, \mathbf{e}_y\}$. The cross product $\mathbf{e}_z = \mathbf{e}_x \times \mathbf{e}_y$ yields a unit normal to the plane, completing an ortho-normal basis associated to the ambient space.

The position vector of any point P of the axis in the reference shape, the arc length ds, and the unit tangent $\mathbf{l}$ are given by

$$\begin{gathered}\mathbf{r}_0(x) = x\mathbf{e}_x + y(x)\mathbf{e}_y, \quad x_a \leq x \leq x_b,\ \ y(x_a) \leq y \leq y(x_b), \\ ds = \sqrt{\frac{d\mathbf{r}_0(x)}{dx} \cdot \frac{d\mathbf{r}_0(x)}{dx}}\, dx, \quad \mathbf{l}(s) = \frac{d\mathbf{r}_0(x(s))}{dx(s)} \frac{dx(s)}{ds} = \frac{d\mathbf{r}_0(s)}{ds}\end{gathered} \tag{1}$$

Eq. $(1)_2$ provides the curvilinear abscissa s in terms of x and vice-versa, hence all the fields depending on P are functions of either x or s, leading to Eq. $(1)_3$.

The s-derivative of the unit tangents and its unit counterpart are

$$\frac{d\mathbf{l}(s)}{ds} = \frac{d\mathbf{l}(x(s))}{dx(s)}\frac{dx(s)}{ds} =: k(s)\mathbf{m}(s), \quad \mathbf{m}(s) = \frac{1}{k(s)}\frac{d\mathbf{l}(s)}{ds} \tag{2}$$

k being the axis curvature at P. Since the axis is plane, the Frénet-Serret local basis is $\{\mathbf{l}, \mathbf{m}, \mathbf{n}\}$, with $\mathbf{n} = \mathbf{l} \times \mathbf{m} = \pm \mathbf{e}_z$ (the sign depends on the location of the osculating circle at P). In the reference shape, the cross-sections are orthogonal to the axis, so that any arch infinitesimal element from P is along $\mathbf{l}$ and the corresponding cross-section is spanned by the normal and bi-normal $\mathbf{m}, \mathbf{n}$.

For simplicity, henceforth we think all fields expressed in terms of the intrinsic abscissa s via Eq. $(1)_2$, and omit such dependence if no confusion arises.

2.1. Finite kinematics, balance, linear elasticity

If we admit the cross-sections to undergo only rigid motions, their translation is given by the vector $\mathbf{d}$ (hence, the new position of the axis is $\mathbf{r} = \mathbf{r}_0 + \mathbf{d} \ \forall P$) and their rotation is given by the proper orthogonal tensor $\mathbf{R}$ (hence, their new setting is spanned by $\mathbf{Rm}, \mathbf{Rn} \ \forall P$); these two fields depend on P (i.e., x or s) and on an evolution parameter. If the axis remains in the plane, i) $\mathbf{R}$ is in terms of a single rotation angle ϑ about $\mathbf{n}$, and ii) $\mathbf{d}$ has two components:

$$(\mathbf{R}) = \begin{pmatrix} \cos\vartheta & -\sin\vartheta \\ \sin\vartheta & \cos\vartheta \end{pmatrix}, \qquad \mathbf{d} = u\mathbf{l} + v\mathbf{m} \tag{3}$$

Rigid changes of shape of the entire arch imply that all cross-sections undergo the same motion: thus, $\mathbf{R}$ shall be uniform along the axis, and the tangent to the new axis shall be the $\mathbf{R}$-transformed of $\mathbf{l} \ \forall P$. Thus, strain is naturally defined as the local difference between a generic change of shape and a rigid one. If primes denote s-derivatives, finite strain measures in the actual shape are the vector and skew-symmetric tensor fields $\mathbf{v}, \mathbf{V}$ [46, 47, 48]

$$\mathbf{v} = (\mathbf{r}_0 + \mathbf{d})' - \mathbf{Rl} = \tilde{\varepsilon}(\mathbf{Rl}) + \tilde{\gamma}(\mathbf{Rm}), \quad \mathbf{V} = \mathbf{R}'\mathbf{R}^\top = \tilde{\chi}(\mathbf{Rl} \wedge \mathbf{Rm}) \tag{4}$$

where $\tilde{\varepsilon}$ is the axial stretch, $\tilde{\gamma}$ is the shearing between axis and cross-sections, $\tilde{\chi}$ is the variation of curvature of the axis, and $\wedge$ is the external product, tensor dual of the cross product. Inserting Eq. (3) into Eq. (4) yields

$$\tilde{\varepsilon} = 1 - \cos\vartheta + kv + u', \qquad \tilde{\gamma} = -\sin\vartheta + ku + v', \qquad \tilde{\chi} = \vartheta' \tag{5}$$

Eq. (5) also give the strain components $\varepsilon, \gamma, \chi$ in the reference shape with respect to its local basis $\{\mathbf{l}, \mathbf{m}, \mathbf{n}\}$, since these are the $\mathbf{R}$-pull-back of (4) [46, 47, 48].

The external actions, power duals of the evolutive increments of the kinematic descriptors, are a force vector and a couple skew-symmetric tensor, distributed along the axis (denoted $\mathbf{b}, \mathbf{B}$) and localised at its ends (denoted $\mathbf{f}, \mathbf{F}$). The interactions among parts of the arch, power duals of the evolutive increments of strain, are a vector and a skew-symmetric tensor, denoted $\mathbf{t}, \mathbf{T}$ respectively. All these fields depend on P and the evolution parameter.

Variational arguments, i.e., the vanishing of virtual work on admissible kinematics [48], yield the bulk and boundary balance in the actual shape

$$\begin{gathered} \mathbf{t}' + \mathbf{b} = \mathbf{0}, \qquad \mathbf{T}' + (\mathbf{r}_0 + \mathbf{d})' \times \mathbf{t} + \mathbf{B} = \mathbf{0} \;\; \forall x \in (x_a, x_b), \\ \mathbf{t} = -\mathbf{t}_a,\; \mathbf{T} = -\mathbf{T}_a \;\text{ at } x = x_a, \qquad \mathbf{t} = \mathbf{t}_b,\; \mathbf{T} = \mathbf{T}_b \;\text{ at } x = x_b \end{gathered} \tag{6}$$

Here $\mathbf{T}, \mathbf{B}$ are axial vectors of the relevant skew-symmetric tensors. The inner actions $\mathbf{t}, \mathbf{T}$ can be referred to local bases in the reference or actual shape

$$\mathbf{t} = N\mathbf{l} + Q\mathbf{m} = \tilde{N}(\mathbf{R}\mathbf{l}) + \tilde{Q}(\mathbf{R}\mathbf{m}), \qquad \mathbf{T} = M\mathbf{n} = \tilde{M}(\mathbf{R}\mathbf{n}) \tag{7}$$

with $N, \tilde{N}, Q, \tilde{Q}$ the normal and transverse force, $M, \tilde{M}$ the bending couple. If the external action in the actual shape (including inertia) has components $\tilde{q}_l, \tilde{q}_m, \tilde{q}_n$ on $\{\mathbf{R}\mathbf{l}, \mathbf{R}\mathbf{m}, \mathbf{R}\mathbf{n}\}$, Eq. (7) yield the scalar consequences of Eq. (6)

$$\tilde{N}' - k\tilde{Q} + \tilde{q}_l = 0, \qquad \tilde{Q}' + k\tilde{N} + \tilde{q}_m = 0, \qquad \tilde{M}' - \tilde{N}(\sin\vartheta + \gamma) + \tilde{Q}(\cos\vartheta + \varepsilon) + \tilde{q}_n = 0, \tag{8}$$

the reference curvature k coming from the s-derivatives of the reference triad.

Since we will perform first-order expansions of the field equations, it is sufficient to pose the arch to be linear elastic, the reference shape to represent its natural state, and the inner actions to be uncoupled; then, the first variation of the elastic potential energy with respect to the strain components yields [47]

$$\tilde{N} = EA\tilde{\varepsilon}, \qquad \tilde{Q} = GA_s\tilde{\gamma}, \qquad \tilde{M} = EI\tilde{\chi} \tag{9}$$

with: E, G Young's and transverse elastic moduli; A, A_s, I the cross-section area, shearing area, and second moment of area referred to a principal axis of inertia parallel to $\mathbf{n}$. Eq. (9) hold for compact cross-sections with main dimension small compared to osculating radii [49] and can be given in terms of the reference components N, Q, M (Eq.(7)) and $\varepsilon, \gamma, \chi$ (Eq. (5) and following comment), considering that local bases are $\mathbf{R}$-transformed

$$\begin{aligned} \varepsilon &= N\left(\frac{\cos^2\vartheta}{EA} + \frac{\sin^2\vartheta}{GA_s}\right) + Q\sin\vartheta\cos\vartheta\left(\frac{1}{EA} - \frac{1}{GA_s}\right), \\ \gamma &= Q\left(\frac{\cos^2\vartheta}{GA_s} + \frac{\sin^2\vartheta}{EA}\right) + N\sin\vartheta\cos\vartheta\left(\frac{1}{EA} - \frac{1}{GA_s}\right), \qquad \chi = \frac{M}{EI} \end{aligned} \tag{10}$$

2.2. Non-trivial equilibrium path, adjacent shape

The response to static loads is the solution of the field differential equations (5), (8), (10), plus boundary conditions. If loads are scaled by a multiplier q growing from zero, an equilibrium path is a family of such solutions that, if no buckling occurs, is described by a single-valued function yielding a characteristic strain vs. q. Bar very special cases, a closed form for equilibrium paths is not found and its numerical approximation is highly computing demanding.

In many applications the structural response features 'small' displacements and rotations, thus linearised field equations suffice to look for a germ of the equilibrium path. We then introduce an evolution parameter η (e.g., $\propto q$), $\eta = 0$ identifies the reference shape and as a suffix denotes reference quantities

$$\mathbf{R}_0 = \mathbf{I} \Leftrightarrow \vartheta_0 = 0, \quad \mathbf{d}_0 = \mathbf{0}, \quad N_0 = Q_0 = M_0 = 0 \tag{11}$$

A neighbourhood of the stress-free reference shape is given by an η-linear expansion of Eqs. (5), (8), (10) about $\eta = 0$ [50]; indeed, this equals to investigating non-trivial equilibria consisting of shapes 'near' the reference one:

$$\begin{aligned} &EA(\dot{u}_e' - k\dot{v}_e) = \dot{N}_e, \qquad GA_s(\dot{v}_e' - \dot{\vartheta}_e + k\dot{u}_e) = \dot{Q}_e, \qquad EI\dot{\vartheta}_e' = \dot{M}_e, \\ &\dot{N}_e' - k\dot{Q}_e + \dot{q_{le}} = 0, \qquad \dot{Q}_e' + k\dot{N}_e + \dot{q_{me}} = 0, \qquad \dot{M}_e' + \dot{Q}_e + \dot{q_{ne}} = 0 \end{aligned} \tag{12}$$

Over-dots denote η-derivatives at $\eta = 0$; the suffix e denotes a field at $\eta = 1$, identifying the shape reached when the loads are fully applied in a quasi-static monotonic growth. For the smallness of displacement and rotation, this extremum of the non-trivial equilibrium path is actually adjacent to the reference shape. Tests on the reliability of Eq. (12) for pattern schemes are found in [43].

2.3. Small vibration superposed on the adjacent shape

Let us now pose pose that any function $g = g_e + g_d$, where the subscript d denotes dynamics superposed on the adjacent shape, corresponding to $g_d = 0$. Further, let g_d regularly depend on another evolution parameter β such that $g_d(\beta = 0) = 0$ or $g(\beta = 0) = g_e$; then, we may formally expand g_d in terms of β about $\beta = 0$ and, if over-dots now stand for β-derivatives at $\beta = 0$,

$$g = g_e + \beta \dot{g}_d + o(\beta^2) \tag{13}$$

Applying Eq. (13) to Eqs. (5), (8), (10) yields six first-order ordinary differential equations that keep memory of the adjacent deformed and loaded shape. Let the β-incremental actions be due to a small amplitude harmonic motion with natural angular frequency ω; omitting over-dots for a simpler notation, we get

$$\begin{gathered} u_d' - kv_d + \vartheta_e \vartheta_d = \frac{N_d}{EA} + Q_e \vartheta_d \left(\frac{1}{EA} - \frac{1}{GA_s} \right), \\ v_d' + ku_d - \vartheta_d = \frac{Q_d}{GA_s} + N_e \vartheta_d \left(\frac{1}{EA} - \frac{1}{GA_s} \right), \\ EI\vartheta_d' = M_d \qquad N_d' - kQ_d + \rho A \omega^2 u_d = 0, \qquad Q_d' + kN_d + \rho A \omega^2 v_d = 0, \\ M_d' - N_e(\gamma_d + \vartheta_d) - N_d(\gamma_e + \vartheta_e) + Q_e(\varepsilon_d - \vartheta_e \vartheta_d) + Q_d(1 + \varepsilon_e) + \rho I \omega^2 \vartheta_d = 0 \end{gathered} \tag{14}$$

where ρ is volumic mass. All quantities in Eq. (14), bar the reference curvature k and the arch properties ρ, A, I, are first-order increments: the subscripts e, d refer to the adjacent shape and to its linear dynamics, respectively. Eq. (14) describe linear dynamics of the adjacent shape modulated by the loads on the reference shape. Remark that Eq. (14) are perturbations of field equations derived by variational procedures; assuming the bulk and boundary balance of force and torque as starting points would yield the same governing system, and simplify to those well-documented in the literature in case of no pre-load [51].

3. Small vibration about non-trivial equilibria of parabolic arches

If the axis is a symmetric segment of parabola with span $2l$ along the x-axis and f the keystone height, Fig. 1, its geometry is

$$
\begin{gathered}
\mathbf{r}_0(x)=x\mathbf{e}_x+f\left(1-\frac{x^2}{l^2}\right)\mathbf{e}_y, \quad -l\leq x\leq l, \quad 0\leq y\leq f \\
\frac{d\mathbf{r}_0}{dx}=\mathbf{e}_x-f\frac{2x}{l^2}\mathbf{e}_y, \quad ds=\sqrt{1+\frac{4f^2x^2}{l^4}}dx, \quad \mathbf{l}=\frac{l^2\mathbf{e}_x-2fx\mathbf{e}_y}{\sqrt{l^4+4f^2x^2}}, \\
k=\frac{2fl^4}{(l^4+4f^2x^2)^{3/2}}, \qquad \mathbf{m}=-\frac{2fx\mathbf{e}_x+l^2\mathbf{e}_y}{\sqrt{l^4+4f^2x^2}}, \qquad \mathbf{n}=\mathbf{l}\times\mathbf{m}=-\mathbf{e}_z
\end{gathered}
\tag{15}
$$

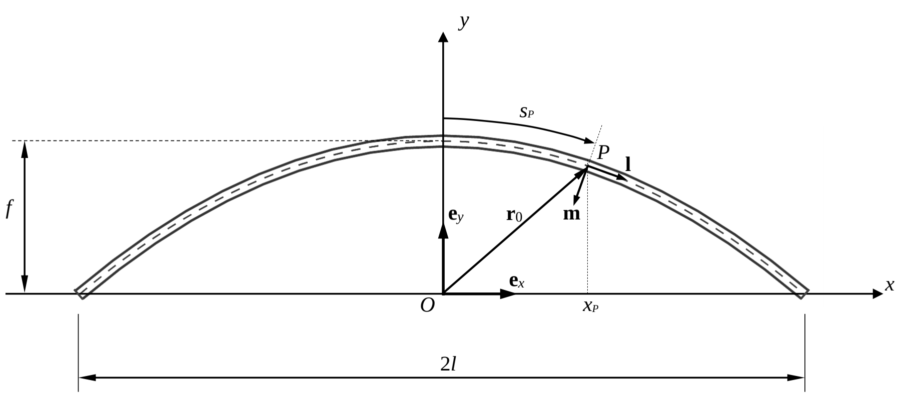

Figure 1: Reference shape of a parabolic arch.

To abstract from particular values of the geometrical and physical parameters, accounting for Eq. (1) we introduce the non-dimensional quantities

$$
\begin{gathered}
(\bar{x},\bar{s},\bar{u},\bar{v},\alpha)=\frac{(x,s,u,v,f)}{l}, \quad \lambda=l\sqrt{\frac{A}{I}}, \quad \bar{A}=\frac{GA_s}{EA}, \quad \bar{\omega}=\omega\lambda l\sqrt{\frac{\rho}{E}}, \\
(\bar{N},\bar{Q},\bar{M})=\frac{(Nl^2,Ql^2,Ml)}{EI}, \quad (\bar{q}_l,\bar{q}_m,\bar{q}_n)=\frac{(q_l l^3,q_m l^3,q_n l^2)}{EI}, \\
\frac{ds}{dx}=\frac{d\bar{s}}{d\bar{x}}=L(\bar{x})=\sqrt{1+4\alpha^2\bar{x}^2}, \qquad \bar{k}(\bar{x})=kl=\frac{2\alpha}{L^3(\bar{x})}.
\end{gathered}
\tag{16}
$$

The adjacent shape is a solution of the system (12), which, by the definitions

(16), admits the matrix representation

$$\frac{d\mathbf{y}_e}{d\bar{x}}=\mathbf{A}_e\mathbf{y}_e+\mathbf{q}_e, \qquad \mathbf{y}_e^T=\left\{\bar{u}_e\ \bar{v}_e\ \vartheta_e\ \bar{N}_e\ \bar{Q}_e\ \bar{M}_e\right\},$$

$$\mathbf{q}_e^T=-L\{0\ 0\ 0\ \bar{q}_{le}\ \bar{q}_{me}\ \bar{q}_{ne}\}, \quad \mathbf{A}_e=L\begin{pmatrix} 0 & k & 0 & \frac{1}{\lambda^2} & 0 & 0 \\ -k & 0 & 1 & 0 & \frac{1}{\bar{A}\lambda^2} & 0 \\ 0 & 0 & 0 & 0 & 0 & 1 \\ 0 & 0 & 0 & 0 & k & 0 \\ 0 & 0 & 0 & -k & 0 & 0 \\ 0 & 0 & 0 & 0 & -1 & 0 \end{pmatrix} \tag{17}$$

Let a parabolic arch in its reference shape undergo a ‘dead’ (invariable in magnitude, direction and orientation) ‘vertical’ η-increment of force $-q\mathbf{e}_y$ uniformly distributed along the span (e.g., gravity). There is no η-increment of external couple, i.e., $q_n = 0 \Rightarrow \bar{q}_{ne} = 0$. Recall that, for simplicity, the overdots denoting η-increments are omitted. Due to the initial curvature, q is not uniform with respect to s and has non-zero components on $\mathbf{l}, \mathbf{m}$ according to

$$-q_e\mathbf{e}_y\,dx = (q_{le}\mathbf{l} + q_{me}\mathbf{m})ds \tag{18}$$

Eqs. (16) yield their non-dimensional counterpart; since q keeps its direction, it is always represented by the components in Eq. (18) when searching equilibria.

The solution of the system in Eq. (17) has the form [52, 53]

$$\mathbf{y}_e(\bar{x}) = \mathbf{Y}_e(\bar{x})\left[\mathbf{y}_e(\bar{x}_0) + \int_0^{\bar{x}} \mathbf{Y}_e^{-1}(\xi)\,\mathbf{q}_e(\xi)\,d\xi\right] \tag{19}$$

where $\mathbf{Y}_e(\bar{x})$ is the principal matrix (*matricant* [54], *transfer matrix* [55]) of the homogeneous Eq. (17) about $\bar{x} = 0$. Its entries in integral form are in [56] for generic arches, in [42] for uniform parabolic ones; variable cross-sections are investigated in [45]. The state vector $\mathbf{y}_e$ in Eq. (19) accounts for distributed actions; concentrated ones were treated in [42] via local continuity and balance.

Since the load is ‘dead’, it will not appear in the field equations for small vibration directly, but via the non-trivial equilibrium path affecting Eq. (14).

By Eqs. (16) we write in matrix form also the system of Eqs. (14), describing the non-dimensional β-first-order harmonic motion:

$$\frac{d\mathbf{y}_d}{d\bar{x}} = \mathbf{A}_d\mathbf{y}_d\,, \qquad \mathbf{y}_d = \left\{\bar{u}_d\ \bar{v}_d\ \vartheta_d\ \bar{N}_d\ \bar{Q}_d\ \bar{M}_d\right\}^T,$$

$$\frac{\mathbf{A}_d}{L} = \begin{pmatrix} 0 & \bar{k} & A_{d13} & \dfrac{1}{\lambda^2} & 0 & 0 \\ -\bar{k} & 0 & A_{d23} & 0 & \dfrac{1}{\bar{A}\lambda^2} & 0 \\ 0 & 0 & 0 & 0 & 0 & 1 \\ -\bar{\omega}^2 & 0 & 0 & 0 & \bar{k} & 0 \\ 0 & -\bar{\omega}^2 & 0 & -\bar{k} & 0 & 0 \\ 0 & 0 & A_{d63} & A_{d64} & A_{d65} & 0 \end{pmatrix}$$

$$A_{d13} = \frac{\bar{Q}_e}{\lambda^2}\left(1 - \frac{1}{\bar{A}}\right) - \vartheta_e, \quad A_{d23} = \frac{\bar{N}_e}{\lambda^2}\left(1 - \frac{1}{\bar{A}}\right) + 1,$$

$$A_{d63} = \bar{N}_e\left[\frac{\bar{N}_e}{\lambda^2}\left(1 - \frac{1}{\bar{A}}\right) + 1\right] - \bar{Q}_e\left[\frac{\bar{Q}_e}{\lambda^2}\left(1 - \frac{1}{\bar{A}}\right) - \vartheta_e\right] - \frac{\bar{\omega}^2}{\lambda^2},$$

$$A_{d64} = -A_{d13}, \quad A_{d65} = -A_{d23} \tag{20}$$

The entry A_{d63} of the state evolution matrix $\mathbf{A}_d$ in Eq. (20) contains the squares of the inner normal and shearing force in the non-trivial equilibrium path $\bar{N}_e, \bar{Q}_e$. One might ask if squares of first-order increments with respect to $\eta \propto q$ should be neglected. However, Eq. (20) describe a perturbation in terms of β that is independent of η (check Eq. (13)); thus, when dealing with the quantities with subscript d, those with subscript e must be considered as evaluated constants, and their squares do not imply any methodological or numerical error.

In a homogeneous arch the physical and geometrical parameters are uniform, yet the terms in Eq. (20) depend on $\bar{x}$ and $\mathbf{A}_d$ cannot be reduced to upper-triangular, which would lead to formal successive integrations. Thus, in general Eq. (20) does not have closed-form solutions and we search approximate ones via Peano series [57] and Volterra's multiplicative integral [54, 58], as in [41]:

$$\mathbf{y}_d\,(\bar{x}) = \mathbf{Y}_d(\bar{x}, \bar{x}_0)\mathbf{y}_d(\bar{x}_0), \quad \mathbf{Y}_d(\bar{x}, \bar{x}_0) = \prod_{\imath=1}^{n} \mathbf{Y}_2(\bar{x}_0 + \imath\Delta\bar{x}, \bar{x}_0 + (\imath - 1)\Delta\bar{x}),$$

$$\mathbf{Y}_2(\bar{x}_2, \bar{x}_1) \approx \mathbf{I} + \mathbf{A}_d(\bar{x}_1)(\bar{x}_2 - \bar{x}_1) + \left(\frac{1}{2}\,\frac{d\mathbf{A}_d}{dx}\bigg|_{\bar{x}_1} + \frac{1}{4}\,\frac{d^2\mathbf{A}_d}{dx^2}\bigg|_{\bar{x}_1} + \frac{1}{2}\mathbf{A}_d^2(\bar{x}_1)\right)(\bar{x}_2 - \bar{x}_1)^2 \tag{21}$$

The arch portion $\{\bar{x}, \bar{x}_0\}$ is split into n intervals of equal length $\Delta\bar{x} = (\bar{x} - \bar{x}_0)/n$: as n increases, keeping it large enough for convergence, $\Delta\bar{x} \to 0$ and Eq. (21) turns into Volterra's integral [58]. To apply Eq. $(21)_1$ we choose $\bar{x}_0$ and let the state vector function $\mathbf{y}_d(\bar{x})$ depend on $\mathbf{y}_d(\bar{x}_0)$, considered as a list of unknown parameters. Now, the linear dynamics problem (20) shall be completed by three homogeneous boundary conditions at each arch end:

$$\begin{array}{lcccc} \text{clamped end} & : & \bar{u} = 0, & \bar{v} = 0, & \vartheta = 0, \\ \text{pinned end} & : & \bar{u} = 0, & \bar{v} = 0, & \bar{M} = 0, \\ \text{free end} & : & \bar{N} = 0, & \bar{Q} = 0, & \bar{M} = 0, \end{array} \tag{22}$$

i.e., 6 linear homogeneous equations in the 6 unknowns of the list $\mathbf{y}_d(\bar{x}_0)$:

$$\begin{array}{cccc} \mathbf{T}(\bar{\omega}) & \mathbf{y}_d(\bar{x}_0) & = & \mathbf{0} \\ 6 \times 6 & 6 \times 1 & & 6 \times 1 \end{array} \tag{23}$$

with $\mathbf{T}(\bar{\omega})$ a square matrix of coefficients that depend on the natural angular frequency $\bar{\omega}$. Eq. (23) always admits the trivial solution $\mathbf{y}_d(\bar{x}_0) = \mathbf{0}$, which, however, is not admissible: the state vector in this twice perturbed shape in general does not vanish at an arbitrary point of the axis. Thence, we ask for non-trivial state vectors $\mathbf{y}_d(\bar{x}_0) \neq \mathbf{0}$, which equals to requiring the singularity of $\mathbf{T}(\bar{\omega})$ in terms of the unknown $\bar{\omega}$. We get a highly non-linear equation, the solutions of which are the natural angular frequencies for the arch about the deformed shape, modulated by the initial load and the relevant strain

$$\det[\mathbf{T}(\bar{\omega})] = 0 \Rightarrow \bar{\omega} = \bar{\omega}_\imath, \quad \imath = 1, 2, \ldots \tag{24}$$

4. Effects of a local crack on equilibria and superposed small vibration

If a small plane crack affect the cross-section at the non-dimensional abscissa $\bar{x}_c$, we imagine the arch composed by two regular chunks joined at x_c by a set of springs. Following [7] and similarly to what is done in [40], their compliances depend on the depth of the crack via its complementary strain energy U_c

$$U_c = \int_{A_c} \frac{1}{E'} \left[\left(\sum K_{I\jmath} \right)^2 + \left(\sum K_{II\jmath} \right)^2 \right] dA, \quad c_{\imath\jmath} = \frac{\partial^2 U_c}{\partial \imath \partial \jmath}, \ \imath, \jmath = N, Q, M \tag{25}$$

where: A_c is the damaged cross-section; $E' = E/(1-\nu^2)$, with ν Poisson's ratio, is Young's modulus in plane stress; $K_{I\jmath}, K_{II\jmath}$ are the stress intensity factors in opening and shearing modes, respectively, related to the $\jmath$-th contact action; $c_{\imath\jmath}$ is the compliance of the spring representing the effect of the crack on the $\jmath$-th contact action due to a unit value of the kinematic descriptor dual of the $\imath$-th contact action (respectively, relative axial and transverse displacement, plus rotation between the cross-sections corresponding to the lips of the crack).

Let the undamaged cross-sections be rectangles of height h; the damaged one at $\bar{x}_c$ exhibits a crack of depth a that can be at its opposite sides with respect to the centre of curvature. The crack-related non-dimensional quantities are

$$\begin{gathered}\bar{a} = \frac{a}{h}, \quad \bar{K}_{\imath\jmath} = \frac{K_{\imath\jmath}}{E\sqrt{h}}, \quad \bar{U}_c = \frac{U_c}{hEA}, \quad \left(\bar{c}_{\bar{N}\bar{N}}, \bar{c}_{\bar{Q}\bar{Q}}\right) = \frac{EI\left(c_{NN}, c_{QQ}\right)}{l^3}, \\ \bar{c}_{\bar{M}\bar{M}} = \frac{EIc_{MM}}{l}, \qquad \bar{c}_{\bar{M}\bar{N}} = \bar{c}_{\bar{N}\bar{M}} = \frac{EIc_{MN}}{l^2}\end{gathered} \tag{26}$$

For determining the stress intensity factors to insert in Eqs. (25), (26), we use, as in [45, 42, 43], the numerical shape functions $f_\imath$, $\imath = 1, 2, 3$ provided by [7], which depend on the depth of the crack. If ζ ranges along the non-dimensional crack depth, we get the non-dimensional compliances

$$\begin{gathered}\bar{c}_{\bar{N}\bar{N}} = \frac{4\pi\sqrt{3}(1-\nu^2)}{\lambda^3}\int_0^{\bar{a}} \zeta f_1^2\left(\zeta\right)d\zeta, \quad \bar{c}_{\bar{Q}\bar{Q}} = \frac{16\pi\sqrt{3}(1-\nu)}{\bar{A}^2\lambda^3(1+\nu)}\int_0^{\bar{a}} \zeta f_2^2(\zeta)d\zeta, \\ \bar{c}_{\bar{M}\bar{M}} = \frac{12\pi\sqrt{3}(1-\nu^2)}{\lambda}\int_0^{\bar{a}} \zeta f_3^2\left(\zeta\right)d\zeta, \quad \bar{c}_{\bar{N}\bar{M}} = \frac{12\pi(1-\nu^2)}{\lambda^2}\int_0^{\bar{a}} \zeta f_1\left(\zeta\right)f_3\left(\zeta\right)d\zeta\end{gathered} \tag{27}$$

Even though all $f_\imath$ have the same order of magnitude [7], the powers of the slenderness ratio λ in Eq. (27) provide very different compliances. Indeed, in slender one-dimensional elements λ has order of hundreds, thus the compliances of normal and shearing springs $\approx 10^{-6}$, that of the spring accounting for the coupling of normal and bending actions $\approx 10^{-4}$, and that of the bending spring $\approx 10^{-2}$. This will result in quite different responses of the damaged arch, as our investigation of particular cases will highlight.

Since we will deal only with the non-dimensional quantities (16), (26), (27), we will abuse of notation again and omit over-bars to lighten readability.

At the damaged cross-section, inner actions are balanced for no point loads, and the crack induces a jump of the kinematics descriptors, elastically linked to inner actions. These conditions are written in different triads, since the cross-sections of the crack lips in general undergo different rotations. Without loss in generality, we choose the triad pertaining to the right end of the left chunk (henceforth labelled by the subscript l). To project quantities at the left end of the right chunk (henceforth labelled by the subscript r) onto it, we use a change of basis, which is the transpose of the relative rotation between the left and right crack lips, $\mathbf{R}(\vartheta_l)\mathbf{R}^T(\vartheta_r)=\mathbf{R}(\vartheta_l-\vartheta_r)$. Its transpose for 'small' angles equals the opposite, so jump and balance conditions in the adjacent shape are

$$\begin{gathered}\mathbf{R}\left(\vartheta_r-\vartheta_l\right)\tilde{\mathbf{d}}_r-\tilde{\mathbf{d}}_l=\mathbf{C}^*\tilde{\mathbf{f}}_l \qquad \mathbf{R}\left(\vartheta_r-\vartheta_l\right)\tilde{\mathbf{f}}_r-\tilde{\mathbf{f}}_l=\mathbf{0},\\ \mathbf{C}^*=\begin{pmatrix} c_{NN} & 0 & pc_{NM}\\ 0 & c_{QQ} & 0\\ pc_{NM} & 0 & c_{MM}\end{pmatrix}, \qquad \tilde{\mathbf{f}}=\left\{\tilde{N},\tilde{Q},\tilde{M}\right\}^T\end{gathered} \tag{28}$$

where $\mathbf{C}^*$ is the matrix of the compliances in (27) and $p=\pm1$ is a non-material parameter indicating that the crack is at the top or bottom of the cross-section with respect to the centre of curvature, respectively. Since we write all vector fields in the actual shape with respect to the Frénet-Serret local basis in the reference shape (see Eq. (7)), Eqs. $(28)_{1,2}$ become

$$\begin{gathered}\mathbf{R}(\vartheta_r-\vartheta_l)\mathbf{R}^T(\vartheta_r)\mathbf{d}_r-\mathbf{R}^T(\vartheta_l)\mathbf{d}_l=\mathbf{C}^*\mathbf{R}^T(\vartheta_l)\mathbf{f}_l,\\ \mathbf{R}(\vartheta_r-\vartheta_l)\mathbf{R}^T(\vartheta_r)\mathbf{f}_r=\mathbf{R}^T(\vartheta_l)\mathbf{f}_l\end{gathered} \tag{29}$$

Now, $\mathbf{R}\left(\vartheta_r-\vartheta_l\right)\mathbf{R}^T\left(\vartheta_r\right)=\mathbf{R}^T\left(\vartheta_l\right)$ (in two-dimensional spaces rotations are commutative), thus Eq. (29) in matrix form in terms of the state vector $\mathbf{y}$ is

$$\mathbf{y}_r(x_c)=\mathbf{C}(a,p)\mathbf{y}_l(x_c), \qquad \mathbf{C}\left(a,p\right)=\begin{pmatrix}\mathbf{I} & \mathbf{R}\left(\vartheta_l(x_c)\right)\mathbf{C}^*\mathbf{R}^T\left(\vartheta_l(x_c)\right)\\ \mathbf{0} & \mathbf{I}\end{pmatrix}, \tag{30}$$

where $\mathbf{0},\mathbf{I}$ are the 3×3 null and identity matrices. Eq. (30) is in finite form and holds for any arch configuration, thus we submit it to the same first-order perturbations performed for the field equations and get

$$\mathbf{y}_r(x_c)=\mathbf{C}_e\mathbf{y}_l(x_c), \qquad \mathbf{y}_r(x_c)=\mathbf{C}_d\mathbf{y}_l(x_c) \tag{31}$$

The first Eq. (31) provides jump and balance in the adjacent shape and was provided also in [42]. The second provides jump and balance for the superposed small vibration and is not provided elsewhere; however, $\mathbf{C}_d$ depends on ϑ_d in a rather extensive way that is not worth reporting here for the sake of space.

For both chunks Eq. (19) gives the static solution in terms of the twelve parameters listed in the state vectors $\mathbf{y}_e(x_{0l}), \mathbf{y}_e(x_{0r})$ of two points x_{0l}, x_{0r}. These are uniquely found by imposing boundary (three scalar equations at each end) and jump and balance conditions at x_c (six scalar consequences), yielding 12 physically independent equations. To simplify calculations, though, it is better to choose a point x_0 (with no loss in generality, in the left chunk) and the components of its state vector $\mathbf{y}_{el}(x_0)$ as parameters; then, the whole solution depends on $\mathbf{y}_{el}(x_0)$ by accounting for the jump and balance in Eq. $(31)_1$

$$\mathbf{y}_{er}(x_0) = \mathbf{Y}_e^{-1}(x_c)\left(\mathbf{C}_e\mathbf{Y}_e(x_c)\mathbf{y}_{el}(x_0) + \left(\mathbf{C}_e - \hat{\mathbf{I}}\right)\int_0^{x_c} \mathbf{Y}_e^{-1}(\xi)\,\mathbf{q}_e(\xi)\,d\xi\right) \tag{32}$$

where $\hat{\mathbf{I}}$ is the 6×6 identity and Eqs. (17), (19) were considered. In this way, the solution to the problem is again reduced to imposing the boundary conditions.

To investigate linear dynamics about the adjacent shape, we update the principal matrix for a crack location x_c inside the $\jmath$-th interval $\{x_0, x\}$:

$$\begin{gathered}\mathbf{Y}_d(x, x_0) = \mathbf{Y}_d\left(x, x_0 + \jmath\Delta x\right)\mathbf{Y}_{dc}\mathbf{Y}_d\left(x_0 + (\jmath - 1)\,\Delta x, x_0\right)\\ \mathbf{Y}_{dc} = \mathbf{Y}_2\left(x_0 + \jmath\Delta x, x_c\right)\mathbf{C}_d\mathbf{Y}_2\left(x_c, x_0 + (\jmath - 1)\,\Delta x\right)\end{gathered} \tag{33}$$

where $\mathbf{Y}_2$ is in Eq. (21). Then, operating as before, to ensure non-trivial $\bar{\mathbf{y}}(\bar{x}_0)$, one must solve an eigenvalue problem analogous to Eq. (24) to get the natural angular frequency of the damaged arch about a non-trivial pre-stressed shape.

5. Validation of the model and technique

In this section we provide a couple of validations of our resolution technique: we first investigate the results that we get by the principal matrix when searching the natural angular frequencies of an undamaged parabolic arch: thus, we show that the numerical technique is robust and reliable. In second place, we investigate the modulating effect of a pre-load on the natural angular frequencies of an undamaged parabolic arch, until the critical threshold of static stability is reached and buckling occurs: thus, we show we can describe natural vibration superposed on a non-trivial adjacent shape.

5.1. Free Vibration of Undamaged Arches

It is easy to check that in absence of pre-loads the field equations proposed here reduce to those presented and validated in [41]. We show their validity and that of the proposed solution procedure by numerical comparisons with the results of the well-established finite element formulation for curved beams presented in [59]. The numerical results for different geometric properties are reported in Table 1 for a doubly clamped arch. The arch geometry accounts for different shallowness ratios α and slenderness ratios λ; the cross-section is rectangular, whence the shear-to-normal cross-section area ratio is $\bar{A}=0.1$ which corresponds to an I-profile with wide flanges for Poisson's ratio $\nu \approx 1/3$. The numerical results are obtained for $n=100$ after a convergence analysis.

Table 1: First four natural frequencies of doubly clamped parabolic arches, $\bar{A}=0.1$.

	$\alpha = 0.2$		$\alpha = 0.4$		$\alpha = 0.6$	
λ	[59]	Present	[59]	Present	[59]	Present
15	6.446	6.443	8.093	8.080	6.554	6.540
	9.591	9.576	9.267	9.262	10.960	10.946
	16.569	16.521	14.989	14.944	13.126	13.086
	22.591	22.538	20.793	20.711	18.532	18.428
30	10.692	10.687	10.385	10.364	8.196	8.175
	12.499	12.476	16.419	16.397	16.340	16.275
	23.554	23.475	21.977	21.918	22.990	22.967
	35.122	34.936	31.099	30.924	26.593	26.422
50	13.552	13.525	11.183	11.158	8.736	8.712
	16.126	16.115	20.924	20.853	18.202	18.120
	27.350	27.257	31.342	31.308	30.361	30.145
	41.483	41.236	36.232	36.006	36.992	36.937

Our results well match those of the finite element formulation in [59], providing always lower values with respect to them and with an increasing, however always small, discrepancy with the shallowness ratio α. The discrepancy is slightly affected by the slenderness ratio λ and grows with the frequency order. This is in accord with the physical interpretation provided in [59]; however, since we are interested in the accuracy of our method accounting for various geometrical and constitutive parameters, we are happy with the obtained results.

5.2. Critical Loads

As another validation test of the approach presented here, let us examine the possibility to detect the threshold of static buckling for undamaged parabolic arches under the given initial load. A 'vertical, dead' load of uniform magnitude q_0 with respect to the arch span, according to (18), leads to the following local components in the reference local Frénet-Serret triad

$$q_{le} = \frac{2q_0 x\alpha}{L^2(x)}, \quad q_{me} = \frac{q_0}{L^2(x)} \tag{34}$$

Letting the load magnitude be the tuning parameter, the vanishing of the vibration frequencies is an indicator of buckling: thus, we let $\omega = 0$ and look for the value q_0 for which non-trivial solutions exist, yielding the critical loads.

Both for the purpose of comparison, and to test the present approach in a limit case, we let $\lambda \to \infty$, which corresponds to a purely flexible arch. We compare the results obtained by the technique presented here with those in: [44], obtained by either differential quadrature (DQM) and finite elements (FEM) using a commercial software package; the well-known monograph by Timoshenko and Gere [60]. In Tab. 2 we see that the results are well in agreement, thus providing another positive validation of our technique.

6. A direct problem

The validity of the field equations derived here is ensured by both the rigour of each step and a qualitative comparison with some literature [41, 42, 44]. Thus,

Table 2: Critical loads for purely flexible doubly-clamped arches.

α	DQM [44]	FEM [44]	[60]	Present
0.2	7.616	7.617	7.588	7.594
0.4	12.887	12.888	12.625	12.851

we perform some applications: as for a direct problem, we examine the effects of a 'dead' pre-load of uniform magnitude q_0 with respect to the arch span on the natural 'small' transverse vibration frequencies of a doubly-clamped parabolic arch. The non-zero components of the distributed load with respect to the local referential Frénet-Serret triad are found by (18) and expressed by Eq. (34). In order to plot some results, we choose the non-dimensional parameters to have values $\alpha = 0.4, \lambda = 100, \bar{A} = 0.3$, roughly corresponding to a moderately shallow and moderately slender arch with rectangular cross-sections.

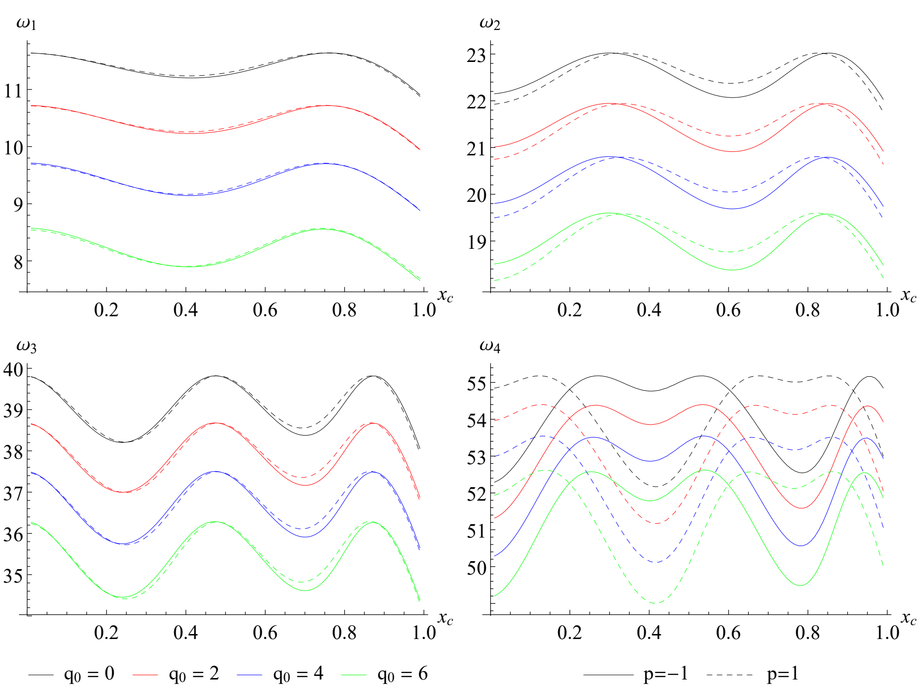

Figure 2: First four frequencies vs. crack location for various pre-loads; $a = 0.5$.

Fig.2 shows how the values of the first four vibration frequencies are affected by a crack located at x_c and by a set of discrete values of the pre-load growing from zero, the latter case indicating an unloaded arch. Remark that only a half of the arch is considered, due to the symmetry of the problem, hence the possible crack locations are $0 \leq x_c \leq 1$. We consider the set of values for q_0 up to approximately one half the critical load, which, as it is well known, corresponds to the value for which the first natural angular frequency vanishes.

We may see that the natural angular frequencies decrease with increasing pre-load, which thus acts as a frequency modulator; this is in accord with the fact that in this case the outer load is brought by the majority of the arch by a compressive normal force. This, as it is well known, reduces the global stiffness via a negative geometric contribution that sums with the structural elastic stiffness; the opposite would hold if the normal force in the largest part of the arch were of traction. This effect is similar at various levels of the external pre-load, as it is apparent in the plots of Fig. 2, though the curves are not exactly shifted, which will be also highlighted below. In addition, each curve providing the natural angular frequency for a given pre-load versus the crack location x_c along the undeformed axis is not monotonic. This also is physically justified: in our model, various x_c imply that the two regular chunks have different lengths, thus different distributions of the inner actions and of the consequent diminution of the global stiffness, directly affecting the natural frequencies. This effect is also reported in some recent literature [40, 41].

On the other hand, it is apparent that the effect of the crack location on opposite sides of the damaged cross-section, parameterized by p, is different for odd and even modes: it is almost unappreciable for odd modes, quite remarkable for even ones. For a better interpretation of this phenomenon, this outcome shall be read along with Fig. 3, where the first two mode shapes for an unloaded arch and the corresponding distribution of normal force and bending moment due to the elastic response of the arch to the axial strains associated to small transverse vibration are provided for $x_c = 0.5, a = 0.5, p = 1$. We remark that such a particular choice does not affect the generality of the results and of

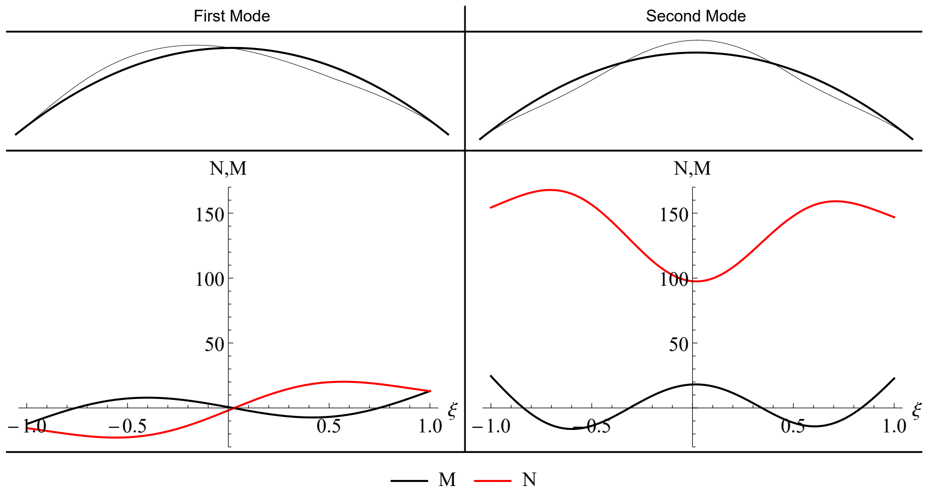

Figure 3: First mode shapes and inner actions; $x_c = 0.5, a = 0.5, p = 1, q_0 = 0$.

their interpretation, since the following remarks hold for arbitrary values of the meaningful parameters. Firstly, we focus on normal force and bending moment only since the compliances of the springs simulating the reduced stiffness of the damaged cross-section, provided in Eq. (27), are coupled for these inner actions (and, indeed, they both depend on elongation parallel to the axis), while the one for shearing force is independent. The normal force and bending moment are normalized by making the integral of the corresponding absolute total displacement of the arch axis equal to unity, and mode shapes are re-scaled for visual purposes. The third and fourth mode shapes are reported in Fig.4 by similar considerations, which have a similar pattern with respect to the first and second. As a rule of thumb, the even mode shapes are almost symmetric, with a slight deviation due to the presence of the local damage; while the odd mode shapes are almost skew-symmetric, with a similar deviation due to the presence of the crack. With reference to Fig.3 and Fig.4, the orders of magnitude of the normal force and bending couple (hence of the relevant distributions of axial strain) are comparable for the first and third modes, while they are remarkably different (one order of difference) for the second and fourth modes; this remark

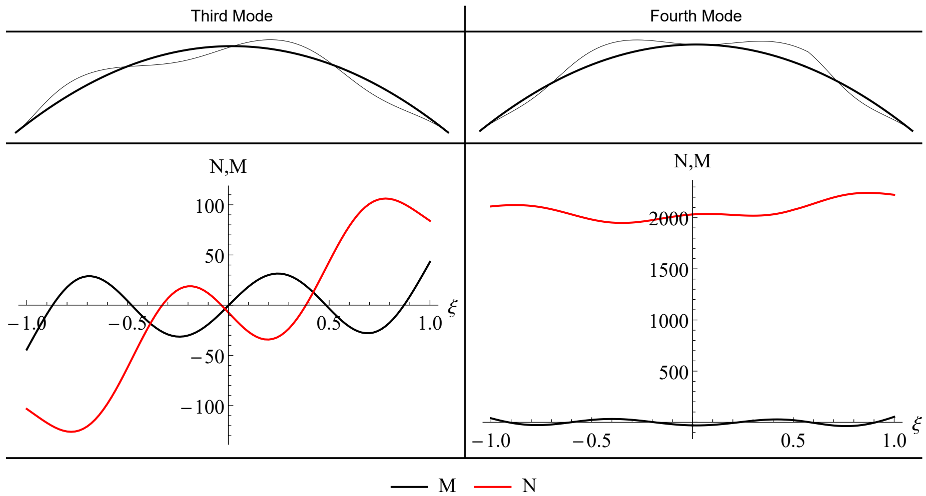

Figure 4: Third and fourth mode shapes and inner actions; $x_c = 0.5, a = 0.5, p = 1, q_0 = 0$.

can be extended to all odd and even modes, respectively. This means that in odd modes the effective compliance is c_{MM} (check the comment after Eq. (27)), the others being negligible in comparison. On the other hand, in even modes the presence of a quite remarkable normal force implies that the coupled compliance $c_{NM} = c_{MN}$, off-diagonal in the matrix representation Eq. (30), is not negligible anymore and its presence softens the structure, representing a compliance added to that due to the bending couple, the latter being dominant in odd modes. Moreover, the off-diagonal compliance is multiplied by the parameter p specifying the location of the crack on opposite sides of the damaged cross-section, hence it is clear why odd modes do not seem affected by p, while the opposite holds for even modes. Another point is that the difference in the orders of magnitude of non-dimensional bending couple and normal force for the fourth mode is an order higher than the second mode. This explains why the effect of damage location on the cross-section is more appraciable for the fourth mode, as seen in Fig.2. We must note that this point shall be read with the assumption of open crack in mind; the the difference may be less depending on the actual shape of the crack or damage and the amplitude of the motion.

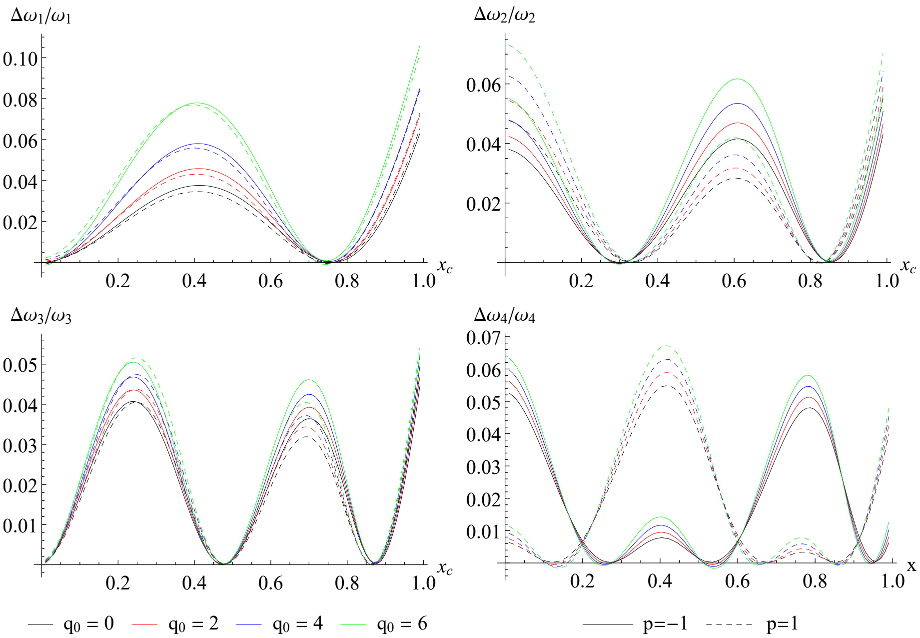

Figure 5: Relative variations of the first four frequencies, $a = 0.5$.

Since the global stiffness of the arch is sensitive to the compliances of the springs simulating the damage, and the latter are strongly affected by the severity of the crack, the modulating effect of the external load might be confused with the softening effect due to the presence of the crack, which reduces in any case the undamaged stiffness. Thus, from the point of view of identification, neglecting a possible pre-load may lead to an overestimation of the severity of the damage. In addition, Fig.5 shows the relative variations of the natural angular frequencies with the load and the crack location: it is apparent that there is some qualitative difference in them with the damage location. This is of applicative interest as these relative variations are usually the data of structural health monitoring process and damage identification procedures using dynamic measurements data.

A better view of this situation is in Fig.6, where the relative variations of natural angular frequencies are provided with respect to the pre-load (left

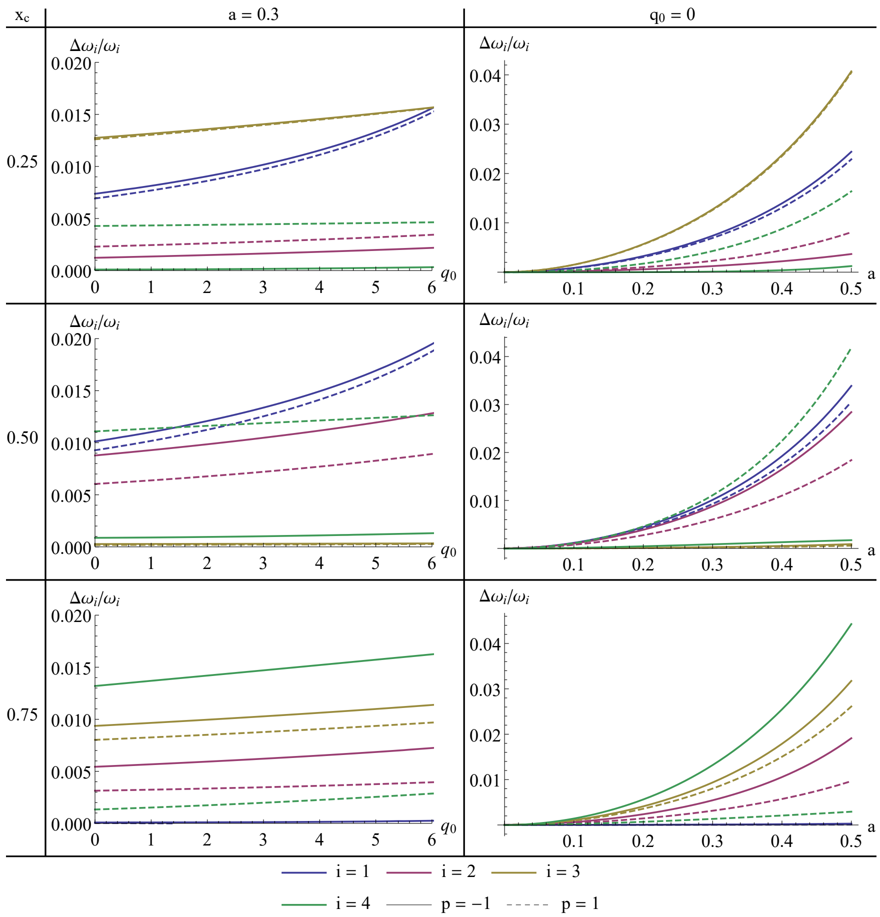

Figure 6: Relative variations of frequencies with pre-load and damage severity.

column) and the damage severity (right column). The damage locations $x_c = 0.25, 0.50, 0.75$ are chosen as *sampling* points as they provide a variety of relative variations of the first four frequencies. Depending on the crack location along the axis, the pre-load affects the frequencies in different ratios, though always lowering them. The increasing damage severity, on the other hand, always alters the frequencies in the same proportion. Relative change of frequency variations with the pre-load resembles the effect of crack location along the axis; therefore, neglecting the pre-load in identification problems may be misleading not only in damage severity, but also on its position along the axis. This is not surprising from the modelling point of view, but it is also expected to have applicative interest since the effects of environmental and operational conditions on health monitoring and identification are evidenced in many papers [23, 61, 62].

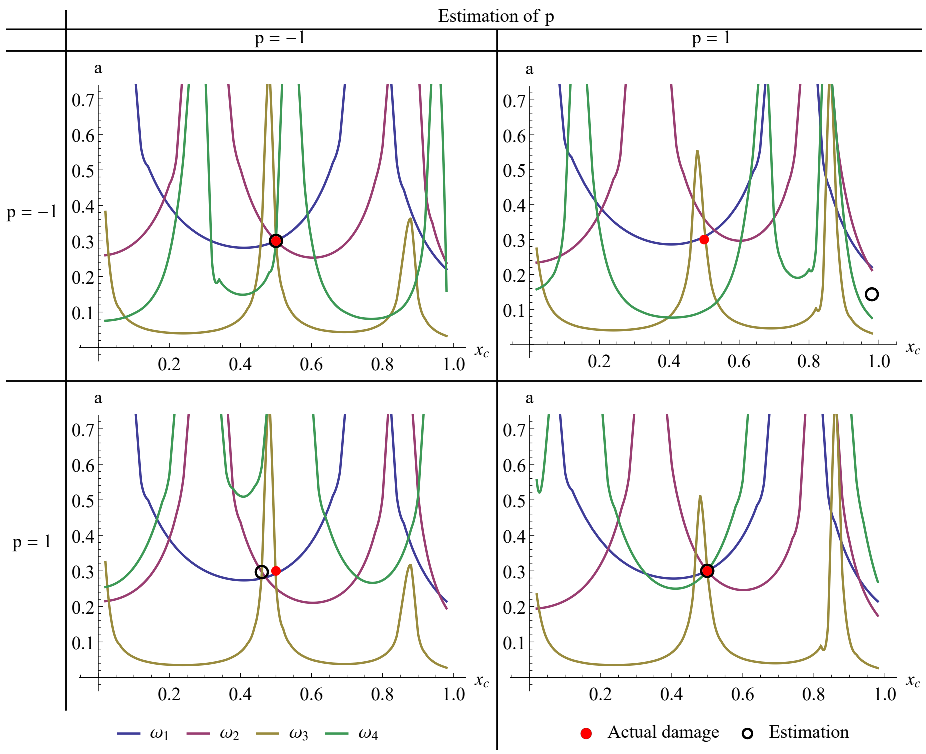

Figure 7: Damage identification by the model with pre-load.

7. An inverse problem

We look for an estimate of the damage parameters in a doubly-clamped parabolic arch by the variations of the first four frequencies. To this aim, we adopt a simple technique, widely used in the literature [28, 36]: for each frequency variation, we find the set of pairs (x_c, a) representing the iso-frequency variation curve $a = f_{\omega_i}(x_c)$, i.e., a curve of constant frequency, calculated by imposing measured variations. In absence of experimental errors, environmental effects, and other uncertainties, it is possible to find a single intersection point when a sufficient number of frequencies are considered. The uniqueness of the solution of the inverse problem, i.e., the possibility to identify the location of the crack in an ideal case, is demonstrated in Fig. 7 using the model with pre-load.

However, in actual applications an optimum point that is closest to all iso-frequency variation curves is looked for by means of a suitable objective function:

$$H_1(x) = \sum_{\substack{i,j=1 \\ i \neq j}}^{4} \left| f_{\omega_i}(x) - f_{\omega_j}(x) \right| \tag{35}$$

Minimizing this function provides an estimation of the crack location along the axis, x_m. Using this value, the damage severity is estimated by another minimization of this second objective function

$$H_2(x) = \sum_{i=1}^{4} \left| f_{\omega_i}(x_m) - a \right| \tag{36}$$

We examine an arch with same geometrical and material parameters in the previous section, with a crack located at $x_c = 0.5$ with a severity $a = 0.3$. We consider both possible crack locations on the cross-section, $p = \mp 1$, and obtain the iso-frequency variation curves with both estimations of the parameter p. In order to see the effects of neglecting the pre-load on the inverse problem, we use the frequency variations of the arch, pre-loaded with $q_0 = 4$; however, we deliberately use the mathematical model with no pre-load. This resembles an actual set of measurements on a pre-loaded arch before and after the damage; however, the mathematical model used in the estimation neglects the pre-load.

Fig.8 shows the iso-frequency variation curves, the location of the actual damage, and its estimation by means of minimization of objective functions given in Eqs. 35 and 36 The points with the colour of the iso-frequency variation curves provide the estimation when the corresponding frequency is left out, which may be needed in case of high noise or other apparent sources of error in specific frequencies [36]. Neglecting the pre-load results in the loss of uniqueness of the solution of the inverse problem and provides different candidate points at

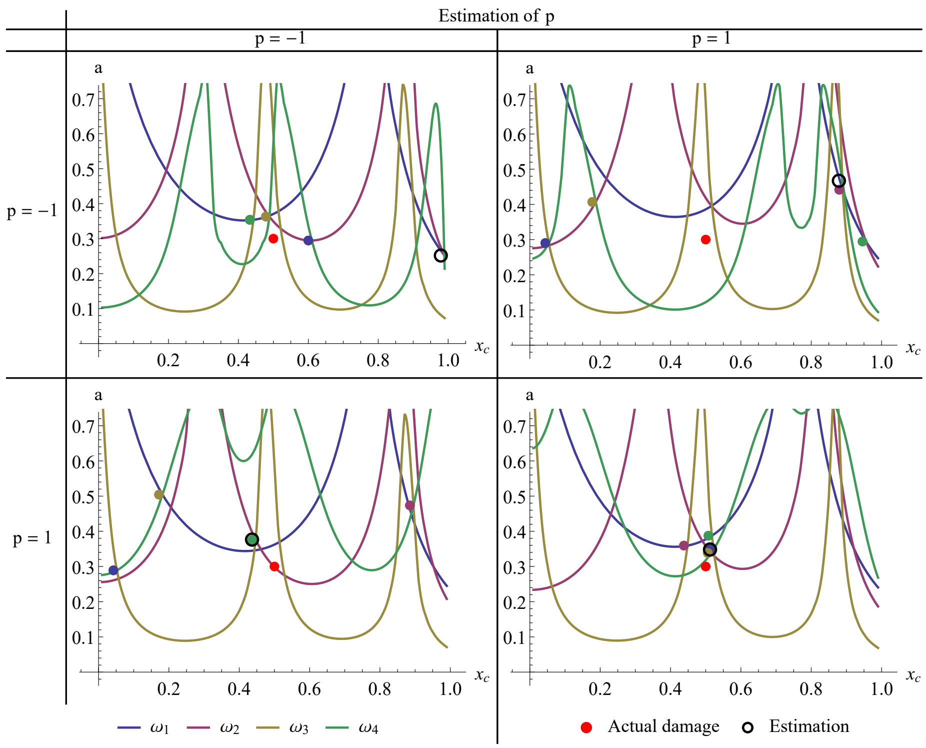

Figure 8: Iso-frequency variation curves and estimation of damage parameters. $q_0 = 4$

which different iso-frequency variation curves intersect which is usual in experimental studies due to uncertainties of different sources. However, in this case the estimation of the damage parameters based on a *pseudo-experiment* is also affected. The importance of the damage location on the cross-section is also evident. We must note that the effect of p may be weakened due to the possible closure of the crack during the initial loading and/or in vibration motion, which calls for a nonlinear modelling of the damage. However, we assume that the crack is always *open* for a linear modelling, as a first step. The top-left and the bottom-right graphs of Fig.8 provide the estimations on damage location along the abscissa and its severity based on correct estimations of its location on the cross-section. For $p = 1$ (bottom-right) we see that the estimations are always close to the actual parameters of the damage: then again, other possible sources of error may add to the inaccuracy of the estimations. This is a clear proof of possible misleading identification due to operational conditions, which can be improved by the enriched model presented herein.

8. Conclusions

We investigated dynamics of initially parabolic arches with local damages under the effect of a vertical 'dead' pre-load, simulating possible permanent weigths on the considered element. Starting from a damaged and unloaded configuration, we performed a first perturbation expansion of the finite field equations, admitting infinitesimal axial displacement and cross-sections rotation. This allowed us to find the linear approximations of the deformed shape and the corresponding internal actions A second perturbation expansion was performed about this deformed and pre-stressed configuration, admitting the incremental displacements and rotation to be infinitesimal again, and harmonic in time.

This two-step perturbation of the field equations, equipped with suitable balance and jump conditions, allowed us to examine the effects of pre-stresses and pre-deformations on small linear transverse vibration of damaged arches. A vertical 'dead' pre-load leads to a decrease in vibration frequencies, as expected. The notable result is that the relative frequency variations depend on the dead load, in addition to the crack location; this disrupts the uniqueness of the inverse problem. In order to evaluate the negative effects of neglecting the pre-load in identification procedures, we adopted a simple technique to find the optimum damage parameters. For this procedure we used the frequency variations of a pre-loaded arch but neglected the effects of the pre-load in the mathematical model, which resembles an actual application of an identification procedure based on frequency shifts on a pre-loaded arch before and after the damage. In addition to the loss of uniqueness of the inverse problem, we found that the estimation of damage parameters may be highly misleading even in the absence of experimental errors, while the correct parameters are recovered for the model accounting for the pre-load. We believe this contribution helps with practical problems of health monitoring, and increase the accuracy of identification procedures by including the operational effects in mathematical modeling.

Acknowledgements

This work was done when U. Eroglu was Visiting Professor at the Dipartimento d'ingegneria strutturale e geotecnica of the University of Rome "La Sapienza", the support of which under the grant 'Professore visitatore 2020' CUP B82F20001090001 is gratefully acknowledged. G. Ruta acknowledges the financial support of the institutional grants RM11916B7ECCFCBF and RM12017294D1B7EF of the University "La Sapienza", Rome, Italy, and of the Italian national research grant PRIN 20177TTP3S-006 from Italian Ministry of University and Research. U. Eroglu and E. Tufekci acknowledge the support of grant by The Scientific and Technological Council of Turkey (TUBITAK) with Project No: 213M608.

References

[1] S. W. Doebling, C. R. Farrar, M. B. Prime, D. W. Shevitz, Damage identification and health monitoring of structural and mechanical systems from changes in their vibration characteristics: a literature review, Los Alamos National Loboratory report LA-13070-MS.

[2] C. R. Farrar, S. W. Doebling, Damage detection II: field applications to large structures. In: J. M. M. Silva and N. M. M. Maia (eds.), Modal analysis and testing, Nato Science Series, Kluwer Academic Publishers, Dordrecht, Netherlands, 1999.

[3] A. D. Dimarogonas, S. A. Paipetis, Analytical methods in rotor dynamics, Applied Science, Paris, 1983.

[4] P. G. Kirshmer, The effect of discontinuities on the natural frequency of beams, Proceeding ASTM 44 (1944) 897–904.

[5] W. J. Thomson, Vibration of slender bars with discontinuities in stiffness, Journal of Applied Mechanics 17 (1949) 203–207.

[6] G. R. Irwin, Analysis of stresses and strains near the end of a crack traversing a plate, Journal of Applied Mechanics 24 (1957) 361–364.

[7] H. Tada, P. C. Paris, G. R. Irwin, The Stress Analysis of Cracks Handbook, 3rd Edition, ASME Press, New York, 2000.

[8] N. Papaeconomou, A. Dimarogonas, Vibration of cracked beams, Computational Mechanics 5 (1989) 88–94.

[9] A. D. Dimarogonas, Buckling of rings and tubes with longitudinal cracks, Mechanics Research Communications 8 (1981) 179–186.

[10] A. D. Dimarogonas, Crack identification in aircraft structures, in: 1st National Aircraft Conf., Athens.

[11] A. D. Dimarogonas, Vibration of cracked structures: A state of the art review, Engineering Fracture Mechanics 55 (5) (1996) 831–857.

[12] C. A. Papadopulos, A. D. Dimarogonas, Coupled longitudinal and bending vibrations of a rotating shaft with an open crack, Journal of Sound and Vibration 117 (1987) 81–93.

[13] C. A. Papadopulos, A. D. Dimarogonas, Coupling of bending and torsional vibration of a cracked timoshenko shaft, Ingenieur-Archiv 57 (1987) 496–505.

[14] C. A. Papadopulos, A. D. Dimarogonas, Stability of cracked rotors in the coupled vibration mode, ASME- 11th Biennal Conference of Mechanical Vibration and Noise, USA (1987) 25–34.

[15] N. Anifantis, A. D. Dimarogonas, Stability of columns with a single crack subjected to follower and vertical loads, International Journal of Solids and Structures 19 (1983) 281–291.

[16] N. Anifantis, A. D. Dimarogonas, Post buckling behavior of transverse cracked columns, Composite Structures 12 (2) (1983) 351–356.

[17] C. Wei, X. Shang, Analysis on nonlinear vibration of breathing cracked beam, Journal of Sound and Vibration 461 (2019) 114901.

[18] S. Caddemi, A. Morassi, Multi-cracked euler–bernoulli beams: Mathematical modeling and exact solutions, International Journal of Solids and Structures 50 (2013) 944–956.

[19] S. Caddemi, I. Calio, F. Cannizzaro, The dynamic stiffness matrix (DSM) of axially loaded multi-cracked frames, Mechanics Research Communications 84 (2017) 90–97.

[20] U. Eroglu, E. Tufekci, Exact solution based finite element formulation of cracked beams for crack detection, International Journal of Solids and Structures 96 (2016) 240–253.

[21] U. Eroglu, E. Tufekci, Free vibration of damaged frame structures considering the effects of axial extension, shear deformation and rotatory inertia: Exact solution, International Journal of Structural Stability and Dynamics 17 (10) (2017) 1750111.

[22] S. Chinchalkar, Determination of crack location in beams using natural frequencies, Journal of Sound and Vibration 247 (3) (2001) 417 – 429.

[23] R. Hou, Y. Xia, Review on the new development of vibration-based damage identification for civil engineering structures: 20102019, Journal of Sound and Vibration 491 (2021) 115741.

[24] S. S. Antman, The Theory of Rods, Springer, Berlin, 1973.

[25] S. Antman, Nonlinear problems of elasticity, Springer-Verlag, New York, 1995.

[26] M. Krawczuk, W. Ostachowicz, Natural Vibrations of a Clamped-Clamped Arch With an Open Transverse Crack, Journal of Vibration and Acoustics 119 (2) (1997) 145–151.

[27] M. N. Cerri, G. C. Ruta, Detection of localised damage in plane circular arches by frequency data, Journal of Sound and Vibration 270 (2004) 39–59.

[28] M. N. Cerri, M. Dilena, G. Ruta, Vibration and damage detection in undamaged and cracked circular arches: experimental and analytical results, Journal of Sound and Vibration 314 (2008) 83–94.

[29] E. Viola, E. Artioli, M. Dilena, Analytical and differential quadrature results for vibration analysis of damaged circular arches, Journal of Sound and Vibration 288 (4) (2005) 887–906.

[30] E. Viola, M. Dilena, F. Tornabene, Analytical and numerical results for vibration analysis of multi-stepped and multi-damaged circular arches, Journal of Sound and Vibration 299 (1) (2007) 143–163.

[31] C. Karaagac, H. Ozturk, M. Sabuncu, Crack effects on the in-plane static and dynamic stabilities of a curved beam with an edge crack, Journal of Sound and Vibration 330 (8) (2011) 1718 – 1736.

[32] H. G. W.H. Müller, G. Herrmann, A note on curved cracked beams, International Journal of Solids and Structures 30 (1993) 1527 – 1532.

[33] I. Caliò, A. Greco, D. D'Urso, Structural models for the evaluation of eigenproperties in damaged spatial arches: a critical appraisal, Archive of Applied Mechanics 86 (11) (2016) 1853–1867.

[34] I. Caliò, D. D'Urso, A. Greco, The influence of damage on the eigenproperties of timoshenko spatial arches, Computers and Structures 190 (2017) 13–24.

[35] F. Cannizzaro, A. Greco, S. Caddemi, I. Caliò, Closed form solutions of a multi-cracked circular arch under static loads, International Journal of Solids and Structures 121 (2017) 191–200.

[36] A. Pau, A. Greco, F. Vestroni, Numerical and experimental detection of concentrated damage in parabolic arch by measured frequency variations, Journal of Vibration and Control 17 (4) (2010) 605–614.

[37] A. Greco, A. Pau, Detection of a concentrated damage in a parabolic arch by measured static displacements, Structural Engineering and Mechanics 39 (6) (2011) 751–765.

[38] M. Zare, Free in-plane vibration of cracked curved beams: Experimental, analytical, and numerical analyses, Proceedings of the Institution of Mechanical Engineers, Part C: Journal of Mechanical Engineering Science 233 (3) (2019) 928–946.

[39] A. Greco, D. D'Urso, F. Cannizzaro, A. Pluchino, Damage identification on spatial timoshenko arches by means of genetic algorithms, Mechanical Systems and Signal Processing 105 (2018) 51–67.

[40] U. Eroglu, E. Tufekci, Crack modeling and identification in curved beams using differential evolution, International Journal of Mechanical Sciences 131-132 (2017) 435–450.

[41] U. Eroglu, G. Ruta, E. Tufekci, Natural frequencies of parabolic arches with a single crack on opposite cross-section sides, Journal of Vibration and Control 25 (7) (2019) 1313–1325.

[42] U. Eroglu, A. Paolone, G. Ruta, E. Tufekci, Exact closed-form static solutions for parabolic arches with concentrated damage, Archive of Applied Mechanics 90 (2020) 673–689.

[43] U. Eroglu, G. Ruta, A. Paolone, E. Tufekci, Buckling and Post-Buckling of Parabolic Arches with Local Damage, in: Modern Trends in Structural and Solid Mechanics 1, eds. N. Challamel, J. Kaplunov, I. Takewaki, ISTE-Wiley, London UK, Hoboken USA, 2021.

[44] U. Eroglu, G. Ruta, Fundamental frequencies and buckling in pre-stressed parabolic arches, Journal of Sound and Vibration 435 (2018) 104–118.

[45] U. Eroglu, G. Ruta, Closed-form solutions for elastic tapered parabolic arches under uniform thermal gradients, Meccanica 55 (2020) 1135–1152.

[46] S. S. Antman, The Theory of Rods, Springer, Berlin, 1973, pp. 641–703.

[47] S. S. Antman, Nonlinear problems of elasticity, Springer-Verlag, New York, 1995.

[48] M. Pignataro, N. Rizzi, G. Ruta, A beam model for the flexural-torsional buckling of thin-walled members, Thin Walled Structures 46 (2008) 816–822.

[49] S. Timoshenko, J. N. Goodier, Theory of Elasticity, 2nd Edition, McGraw Hill, New York, 1951.

[50] L. A. Piganatro M., Rizzi N., Stability, bifurcation and post-critical behaviour of elastic structures, Elsevier, Amsterdam, 1991.

[51] E. Tufekci, A. Arpaci, Exact solution of in-plane vibrations of circular arches with account taken of axial extension, transverse shear and rotatory inertia effects, Journal of Sound and Vibration 1209 (1998) 845–856.

[52] J. H. Hubbard, B. H. West, Differential Equations. In: A dynamical systems approach: higher dimensional systems, no. 18 in Texts in Applied Mathematics, Springer-Verlag, 1995.

[53] E. Tufekci, U. Eroglu, S. A. Aya, A new two-noded curved beam finite element formulation based on exact solution, Engineering with Computers 33 (2) (2017) 261–273.

[54] M. C. Pease, Methods of Matrix Algebra, Academic Press, New York, 1965.

[55] E. Pestel, F. Leckie, Matrix methods in elastomechanics, McGraw-Hill, 1963.

[56] E. Tufekci, A. Arpaci, Analytical solutions of in-plane static problems for non-uniform curved beams including axial and shear deformations, Structural Engineering and Mechanics 22 (2) (2006) 131–150.

[57] G. Peano, Intégration par séries des équations différentielles linéaires, Mathematische Annalen 32 (3) (1888) 450–456.

[58] A. Slavik, Product Integration, Its History and Applications, Matfyz Press, Prague, 2007.

[59] U. Eroglu, E. Tufekci, A new finite element formulation for free vibrations of planar curved beams, Mechanics Based Design of Structures and Machines 46 (6) (2018) 730–750. arXiv:https://doi.org/10.1080/15397734.2018.1456343, doi:10.1080/15397734.2018.1456343.
URL https://doi.org/10.1080/15397734.2018.1456343

[60] G. J. Timoshenko S.P.., Theory of elastic stability, McGraw-Hill, New York, 1961.

[61] Y. An, E. Chatzi, S.-H. Sim, S. Laflamme, B. Blachowski, J. Ou, Recent progress and future trends on damage identification methods for bridge structures, Structural Control and Health Monitoring 26 (10) (2019) e2416, e2416 STC-18-0435.R3.

[62] N. Dervilis, K. Worden, E. Cross, On robust regression analysis as a means of exploring environmental and operational conditions for shm data, Journal of Sound and Vibration 347 (2015) 279–296.